PROCEEDINGS OF SCIENCE

Recent Belle II results on electroweak penguins

Eldar Ganiev

DESY,
Hamburg, Germany

E-mail: eldar.ganiev@desy.de

We report on the recent measurements of electroweak and radiative penguin B decays at the Belle II experiment. We use samples of electron-positron collisions collected at the $\Upsilon(4S)$ resonance. We present the measurement of the branching fractions of $B^{+/0} \to K^*(892)^{+/0}\ell^+\ell^-$ ($\ell = e, \mu$), $B^{+/0} \to K^{+/0}J/\psi$, and $B^{+/0} \to X_s\gamma$ decays in the data corresponding to 189 fb^{-1} of integrated luminosity. We also present a search of $B^+ \to K^+\nu\bar{\nu}$ decay in the data corresponding to 63 fb^{-1} of integrated luminosity.

41st International Conference on High Energy physics - ICHEP2022
6-13 July, 2022
Bologna, Italy

1. Introduction

The flavor-changing neutral-current transitions, such as $b \to s$, are suppressed in the standard model. Therefore, the rates of decays mediated by the $b \to s$ transitions are predicted to be relatively low $\sim 10^{-7}$–10^{-5} for exclusive modes and $\sim 10^{-4}$ for inclusive modes in the standard model. However, the presence of non-standard-model particles can enhance the rates. Therefore, the study of $b \to s$ transitions in the Belle II experiment is particularly attractive to explore the physics beyond the standard model.

Belle II is a magnetic spectrometer [1, 2], designed to reconstruct the products of electron-positron collisions produced by the SuperKEKB asymmetric-energy collider [3], located at the KEK laboratory, Japan. The Belle II detector started its collision operations on March 11, 2019. The samples of electron-positron collisions collected at the $\Upsilon(4S)$ resonance used in this work corresponds to the integrated luminosities of 63 fb^{-1} and 189 fb^{-1} [4].

The study of the lepton-flavor universality (LFU) is a powerful probe of the non-standard-model physics. Previous LHCb and Belle measurements show some hints of the LFU violation in $B \to K^{(*)}\ell\ell$ decays. Belle II experiment will provide an independent test of the LFU anomalies once it collects a sample corresponding to a few ab^{-1} of integrated luminosity. In a meanwhile, we are preparing for the LFU-violation test by measuring the branching fractions of $B^{+/0} \to K^*(892)^{+/0}\ell^+\ell^-$ ($\ell = e, \mu$) and $B^{+/0} \to K^{+/0}J/\psi$ decays. We also search for the $B^+ \to K^+\nu\bar{\nu}$ decay, which could be sensitive to the same new-physics contributions, as $B \to K^{(*)}\ell\ell$ decays. We measure the $B \to X_s\gamma$ decay, which is not related to the LFU violation, but is potential to probe the physics beyond the standard model.

In most of analyses, to distinguish between signal and background coming from other B-meson decays and the production of light-quark pairs $e^+e^- \to q\overline{q}$ ($q = u, d, s, c$) (continuum events), we use two variables: beam-energy-constrained mass and energy difference, defined as $\mathrm{M_{bc}} \equiv \sqrt{s/(4c^4) - (p^*_B/c)^2}$ and $\Delta E \equiv E^*_B - \sqrt{s}/2$, where $\sqrt{s}/2$ is the half of the collision energy, E^*_B and p^*_B are the reconstructed energy and momentum of B-meson candidates, all in the $\Upsilon(4S)$ frame. In what follows, charge-conjugate modes are implied, K^* indicates the $K^*(892)^+$ and $K^*(892)^0$ mesons, K indicates the K^+ and K^0_S mesons, and B indicates the B^+ and B^0 mesons, except when otherwise stated.

2. Measurement of the branching fraction of $B \to K^*\ell^+\ell^-$ decays

We form K^* candidates by combining a kaon (K^+ or K^0_S) with a pion (π^0 or π^+) satisfying kaon- or pion-enriching selection requirement, respectively [5]. To suppress backgrounds coming from charmonium resonances, we exclude the dilepton-invariant mass ranges corresponding to J/ψ and $\psi(2S)$ resonances. The $B \to K^*\gamma(\to e^+e^-)$ decays are suppressed by requiring the dilepton mass $\mathrm{M}(e^+e^-) > 0.14$ GeV/c^2. Further, we suppress the background by using a binary boosted decision-tree classifier [6] that makes a non-linear combination of about 10 kinematic, vertex, and event-shape variables. By using simulated samples, the selection on the classifier output is optimized by maximizing the signal significance. After applying the optimized selection, we choose one candidate per event with ΔE closest to zero.

We determine signal yields from maximum likelihood fits of the unbinned ΔE and M_{bc} distributions of candidates restricted to the $M_{bc} > 5.2$ GeV/c^2 and -0.15 < ΔE < 0.1 GeV region. Fit models are obtained empirically from simulation. Examples of the M_{bc} distributions with fit projections overlaid are shown in Fig. 1.

We determine branching fractions as $\mathcal{B} = N/(2\varepsilon f^{+-(00)} N_{B\overline{B}})$, where N is the signal yield obtained from the fit, ε is the reconstruction and selection efficiency corrected for data-simulation discrepancies, $f^{+-(00)}$ is the branching fraction of $\mathcal{B}(\Upsilon(4S) \to B^+B^-(B^0\overline{B^0}))$, and $N_{B\overline{B}} = 197{\times}10^6$ is the number of $B\overline{B}$ pairs derived from a data-driven subtraction of the non-resonant contribution from the recorded data. We use $f^{+-} = (51.4 \pm 0.6)\%$ and $f^{00} = (48.6 \pm 0.6)\%$ for charged and neutral B mesons [9].

After taking into account the systematic uncertainties, the measured branching fractions for the entire q^2 region, excluding the J/ψ and $\psi(2S)$ resonances and low q^2 region, are $\mathcal{B}(B \to K^*\mu^+\mu^-) = (1.19 \pm 0.31^{+0.08}_{-0.07}) \times 10^{-6}$ and $\mathcal{B}(B \to K^*e^+e^-) = (1.42 \pm 0.48 \pm 0.09) \times 10^{-6}$. Here, the first and second uncertainties are statistical and systematic, respectively. The precision of the result is similar for electron and muon channels, and is limited by the sample size.

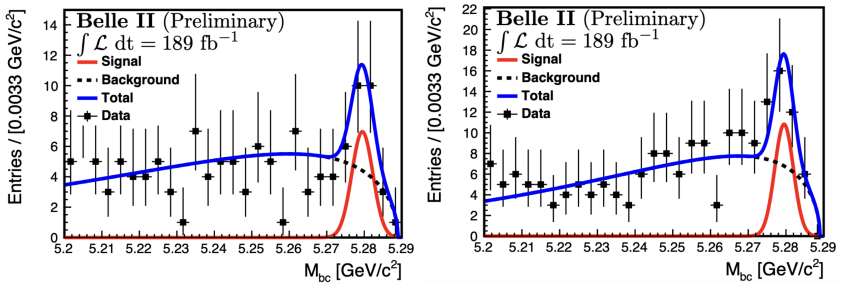

Figure 1: Distributions of M_{bc} for (left) $B \to K^*e^+e^-$ and (right) $B \to K^*\mu^+\mu^-$ candidates reconstructed in 2019–2021 Belle II data. The projections of unbinned maximum likelihood fits are overlaid.

3. Measurement of the branching fraction of $B \to KJ/\psi$ decays

The $B \to KJ/\psi$ decay is not mediated by the $b \to s$ current but it is an essential control channel for the $B \to K\ell^+\ell^-$ decay study. First, we select K, μ, and e candidates by applying kaon-, muon-, and electron-enriching selection, respectively [7]. We then combine a pair of oppositely-charged leptons to form a J/ψ candidate. The invariant mass of the J/ψ candidate is required within (2.91, 3.19) GeV/c^2 and (2.96, 3.19) GeV/c^2 range for the electron and muon channel, respectively. Finally, we combine J/ψ and K candidates in a kinematic fit to reconstruct B candidates. In case of multiple candidates, B candidate with the highest χ^2 probability of the kinematic fit is chosen.

We determine signal yields from maximum likelihood fits of the unbinned ΔE and M_{bc} distributions of candidates restricted to the $M_{bc} > 5.2$ GeV/c^2 and -0.1 < ΔE < 0.2 GeV region. Fit models are obtained empirically from simulation. Examples of the ΔE distributions with fit projections overlaid are shown in Fig. 2. By using same formula as discussed in Section 2 we calculate the branching fractions and determine the branching fraction ratios $R_K(J/\psi) = \frac{\mathcal{B}(B\to KJ/\psi(\to\mu^+\mu^-)}{\mathcal{B}(B\to KJ/\psi(\to e^+e^-)}$. The results are $R_{K^+}(J/\psi) = 1.009 \pm 0.022 \pm 0.008$ and $R_{K^0_S}(J/\psi) = 1.042 \pm 0.042 \pm 0.008$. The

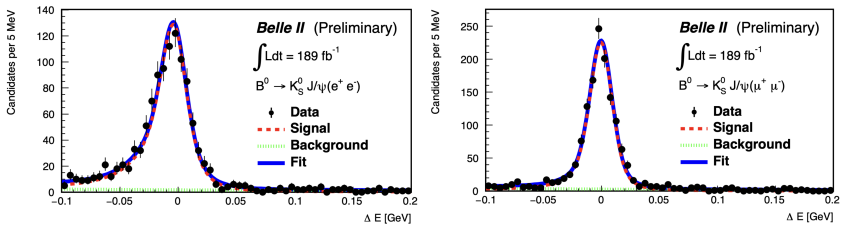

Figure 2: Distributions of ΔE for (left) $B^0 \to K^0_S J/\psi(\to e^+e^-)$ and (right) $B^0 \to K^0_S J/\psi(\to \mu^+\mu^-)$ candidates reconstructed in 2019–2021 Belle II data. The fit projections are overlaid.

first contribution to the uncertainty is statistical, the second is systematic. The precision of the $R_K(J/\psi)$ result is dominated by the statistical uncertainty.

4. Search for the $B^+ \to K^+\nu\bar{\nu}$ decay by using the inclusive-tagging method

We search for $B+ \to K^+\nu\bar{\nu}$ decays by using the inclusive-tagging method [8]. First, we choose a single charged kaon candidate by requiring a charged particle with the highest transverse momentum p_T in the event. We then combine signal discriminating variables in two subsequent multivariate classifiers BDT_1 and BDT_2. The BDT_2 classifier is trained on simulated samples that are restricted to the high values of BDT_1 output. This procedure helps to keep the computational effort low, while significantly increasing the discrimination power. We then restrict the sample to BDT_2 output > 0.93.

We extract the signal yield by performing a binned maximum likelihood fit of p_T and BDT_2 output distributions obtained in the $\Upsilon(4S)$ data and data collected 60 MeV below the $\Upsilon(4S)$ resonance corresponding to 63 fb^{-1} and 9 fb^{-1} of integrated luminosity, respectively. The histogram templates are taken from simulation. We include systematic uncertainties as nuisance parameters in the fit. The leading systematic source is obtained to stem from the normalization of the individual background contributions. The Figure 3 shows the obtained fit yields in bins of p_T and BDT_2 output in comparison with the data. No significant signal is observed. We set an upper limit on the branching ratio using CL_s method. The branching fraction is determined to be $\mathcal{B}(B^+ \to K^+\nu\bar{\nu}) < (4.1 \pm 0.5) \times 10^{-5}$ at a 90% confidence level.

5. Measurement of the inclusive branching fraction of $B \to X_s\gamma$ decay by using the hadronic-tagging method

We measure the photon-energy spectrum in radiative B-meson decays into inclusive final states involving a strange hadron and a photon [11]. In the study, the $B \to X_s\gamma$ and $B \to K^*\gamma$ signal simulations are combined using a hybrid model. First, in each event, one B-meson candidate is fully reconstructed using the full-event-interpretation algorithm (FEI) [10], which reconstructs hadronic B decays from thousands of sub-decay chains. The reconstructed B candidate is used as a tag for the recoiling signal B-meson candidate. The sample is then restricted to the tag-side B-meson candidates satisfying $\mathrm{M_{bc}} > 5.245$ GeV/c^2, $|\Delta E| < 0.2$ GeV, and FEI output > 0.001.

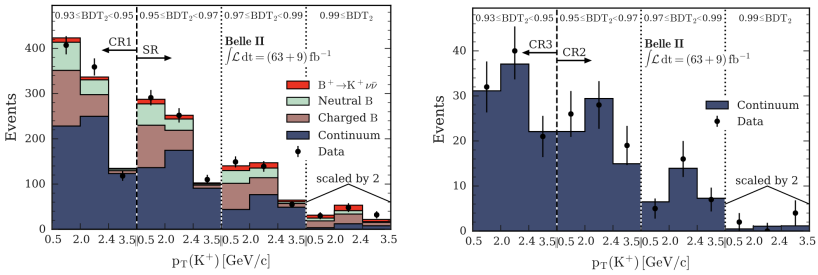

Figure 3: Yields obtained in the bins of $p_{\mathrm{T}}(K^+)$ and BDT_2 in (left) $\Upsilon(4S)$ data and (right) data collected 60 MeV below the $\Upsilon(4S)$ resonance. The expected yields estimated by the fit are presented too. All yields in the rightmost three bins are scaled by a factor of two.

By using the kinematic properties of the reconstructed tag-side meson and the beam-energy constraint, the photon-candidate energy E_γ^B is inferred in the signal-B-meson rest frame. We consider candidates in the range of $E_\gamma^B > 1.4$ GeV. The highest-energy photon in each event is taken as the signal-photon candidate. We then suppress the photon candidates coming from π^0 and η decays. A multivariate classifier is trained to suppress the $e^+e^- \to q\bar{q}$ events. After all the selection, in case of multiple tag-side B-meson candidates in the event, only the candidate with the highest FEI output is kept.

In data and simulation, we then determine the number of well-reconstructed tag-side B mesons by fitting their $\mathrm{M_{bc}}$ distributions obtained in bins of E_γ^B. The resulting yields obtained in bins of E_γ^B are shown on the left plane of Fig. 4.

We determine the number of $B \to X_s\gamma$ candidates by subtracting E_γ^B distribution obtained in simulation from those obtained in data. We then calculate the partial branching fractions in various E_γ^B intervals as $\frac{1}{\Gamma_B}\frac{\mathrm{d}\Gamma_i}{\mathrm{d}E_\gamma^B} = \frac{\mathcal{U}_i \cdot (N_i^{\mathrm{DATA}} - N_i^{\mathrm{BKG,MC}} - N_i^{B\to X_d\gamma})}{\varepsilon_i \cdot N_B}$, where N_i^{DATA} is the yield extracted from fitting the data distributions, $N_i^{\mathrm{BKG,MC}}$ is the non-$B \to X_s\gamma$ yield expectation extracted from fitting the simulated distributions, $N_i^{B\to X_d\gamma}$ is the number of $B \to X_d\gamma$ events equals to $|V_{td}/V_{ts}| \approx 4.3\%$ [9] of $N^{B\to X_s\gamma}$ assuming the same shape and selection efficiency as $B \to X_s\gamma$, ε_i is the $B \to X_s\gamma$ selection efficiency obtained in the hybrid-model simulated sample, $\mathcal{U}_i$ is the bin-by-bin unfolding factor calculated using the hybrid-model simulated sample, and $N_B = 2 \times (198 \pm 3) \times 10^6$ is the number of B mesons in 189 fb^{-1}. Finally, we assess the main systematic effects, such as coming from the fit model, signal efficiency, limited simulated sample size and others. The right plane of Fig. 4 shows the $B \to X_s\gamma$ branching fractions obtained in various bins of E_γ^B.

The integrated branching ratios for various E_γ^B thresholds are calculated and shown in Table 1. The systematic uncertainties are estimated taking the bin-to-bin correlations into account.

Table 1: Integrated partial branching fractions for three E_γ^B thresholds.

E_γ^B threshold, GeV	$\mathcal{B}(B \to X_s\gamma)$, 10^{-4}
1.8	$3.54 \pm 0.78(\mathrm{stat.}) \pm 0.83(\mathrm{syst.})$
2.0	$3.06 \pm 0.56(\mathrm{stat.}) \pm 0.47(\mathrm{syst.})$
2.1	$2.49 \pm 0.46(\mathrm{stat.}) \pm 0.35(\mathrm{syst.})$

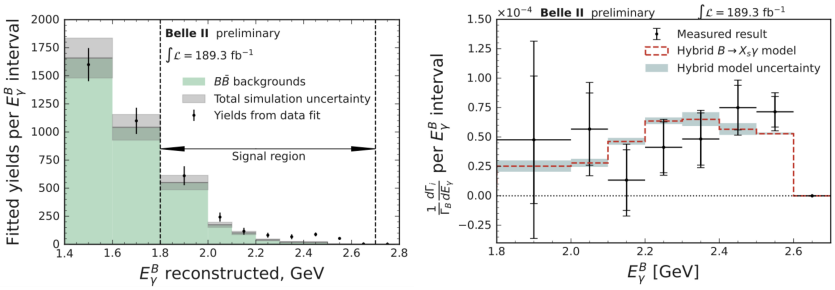

Figure 4: The E_γ^B distribution as the function of (left) resulting yields obtained in the data fit overlaid with the $B\overline{B}$ background yields expected from simulated samples and (right) of measured partial branching fractions $\frac{1}{\Gamma_B}\frac{\mathrm{d}\Gamma_i}{\mathrm{d}E_\gamma^B}$. For the right plot, the outer (inner) error bar shows the total (statistical) uncertainty. The overlaid model and uncertainty corresponds to the hybrid model.

6. Summary

We report on recent measurements of electroweak-penguin and radiative B decays at Belle II. We use data sample of electron-positron collisions collected at the $\Upsilon(4S)$ resonance. We measure branching fractions of $B^{+/0} \to K^*(892)^{+/0}\ell^+\ell^-$ ($\ell = e, \mu$), $B^{+/0} \to K^{+/0}J/\psi$, and $B^{+/0} \to X_s\gamma$ decays in the data corresponding to 189 fb^{-1} of integrated luminosity. By using the data corresponding to 63 fb^{-1} of integrated luminosity, we set an upper limit on the $B^+ \to K^+\nu\bar{\nu}$ branching fraction, as the signal is not observed.

References

[1] Altmannshofer, W. *et al.* (Belle II collaboration), *PTEP* **2019** (2019) no.12, 123C01.

[2] Abe, T. *et al.* (Belle II collaboration), KEK-REPORT-2010-1 (2010) [hep-ex/1011.0352].

[3] Akai, K. *et al.* (SuperKEKB accelerator team), *Nucl. Instrum. Meth.* A **907** (2018) 188.

[4] Abudinén, F. *et al.* (Belle II collaboration), *Chin. Phys. C* **44** (2020) no. 2, 021001.

[5] Abudinén, F. *et al.* (Belle II collaboration), [hep-ex/2206.05946].

[6] Keck, T., [cs.LG/1609.06119].

[7] Abudinén, F. *et al.* (Belle II collaboration), [hep-ex/2207.11275].

[8] Abudinén, F. *et al.* (Belle II collaboration), *Phys. Rev. Lett.* **127**, 181802 (2021).

[9] Zyla. P. A. *et al.* (Particle Data Group), *PTEP* **2020** (2020) no.8, 083C01.

[10] Keck, T. *et al.*, *Comput. Softw. Big Sci* **3** (2019) 6.

[11] Abudinén, F. *et al.* (Belle II collaboration), [hep-ex/2210.10220].